nature computational science

ARTICLES

https://doi.org/10.1038/s43588-022-00198-0

Modeling how antibody responses may determine the efficacy of COVID-19 vaccines

Pranesh Padmanabhan[1]✉, Rajat Desikan[2,4] and Narendra M. Dixit[2,3]✉

Predicting the efficacy of COVID-19 vaccines would aid vaccine development and usage strategies, which is of importance given their limited supplies. Here we develop a multiscale mathematical model that proposes mechanistic links between COVID-19 vaccine efficacies and the neutralizing antibody (NAb) responses they elicit. We hypothesized that the collection of all NAbs would constitute a shape space and that responses of individuals are random samples from this space. We constructed the shape space by analyzing reported in vitro dose–response curves of ~80 NAbs. Sampling NAb subsets from the space, we recapitulated the responses of convalescent patients. We assumed that vaccination would elicit similar NAb responses. We developed a model of within-host SARS-CoV-2 dynamics, applied it to virtual patient populations and, invoking the NAb responses above, predicted vaccine efficacies. Our predictions quantitatively captured the efficacies from clinical trials. Our study thus suggests plausible mechanistic underpinnings of COVID-19 vaccines and generates testable hypotheses for establishing them.

The coronavirus disease 2019 (COVID-19) pandemic has triggered the fastest vaccine development efforts so far, as well as urgent global vaccination rollouts. Yet, limited vaccine supplies are hindering our ability to fight the pandemic[1,2]. Enormous efforts are ongoing to develop new vaccines. As of 14 October 2021, there were 332 vaccine candidates under development, of which 113 were in clinical testing[3]. The ability to predict vaccine efficacies may expedite vaccine development by helping to shortlist promising candidates and/or minimize the subsequent reliance on expensive and time-consuming clinical trials for assessing their efficacies[4]. Simultaneously, it may help identify optimal vaccination strategies[5,6]. For example, although several approved vaccines are administered in two doses separated by a few weeks, it would be useful to know the protection conferred by a single dose, by lower dosages or by doses separated by longer intervals, especially in less vulnerable populations, so as to ease demand[7–9].

Approved COVID-19 vaccines have shown remarkable but varying efficacies in clinical trials, reducing the incidence of 'symptomatic' infections with the wild-type severe acute respiratory syndrome coronavirus 2 (SARS-CoV-2) strain by 62–96% (refs. [7,10–16]). The protection has been argued to be due to neutralizing antibodies (NAbs) elicited by the vaccines. Cellular immunity appears to play a less important role, especially after the recommended doses of the vaccine are administered[10,11,17–22]. The protection due to NAbs is consistent with independent observations, in which higher levels of pre-existing NAbs were correlated with protection and lower risk of infection, respectively, in an early outbreak in a fishery vessel[23] and in a longitudinal study of healthcare workers[24]. Protection from seasonal coronaviruses too has been associated with pre-existing NAbs[25]. Strong statistical correlations have been identified between COVID-19 vaccine efficacies and the NAb responses they elicit[17,18]. An important question that arises is how the NAb responses confer the protection observed. An understanding of the dependence of the level of protection on the NAb titers and their neutralization efficiencies is lacking.

In this Article, we develop a theoretical framework that describes and integrates several key phenomena associated with SARS-CoV-2 infection and vaccination, across length and time scales spanning the range from the workings of individual NAbs to the responses of clinical cohorts to vaccination. The framework employs testable, mechanistic hypotheses and quantitatively predicts the population-level protection conferred by vaccines as a function of the NAb titers they elicit.

Results

Construction of the SARS-CoV-2 NAb landscape. A major challenge to describing the effects of vaccination is the diversity of the NAb responses elicited. The NAb response to primary SARS-CoV-2 infection in unvaccinated individuals is diverse, spanning >1,000-fold variation in Ab titers and in vitro neutralization efficiencies across individuals[26,27]. NAb titers following vaccination have been found to be comparable to those from convalescent patients[10,11,28]. No formalism exists to predict this diversity or its effects on protection. We addressed this challenge by adapting the classic idea of 'shape space', which has aided quantification of the immune repertoire[29], for characterizing NAbs. Accordingly, we sought features (also termed shape parameters) of the NAbs that would predict their neutralization efficiencies. Numerous studies have isolated individual NAbs from patients and assessed their neutralization efficiencies in vitro. We compiled dose–response curves (DRCs) of ~80 NAbs[26,27,30–44] thus isolated and fit them using the median-effect equation[45] (Methods, Supplementary Fig. 1 and Supplementary Data 1). The equation fit the data well (Fig. 1a and Supplementary Fig. 2), indicating that two parameters, the 50% inhibitory concentration (IC_{50}) and the slope (m) of the DRC, were sufficient to characterize the neutralization efficiency of individual NAbs (Fig. 1a and Supplementary Data 1). The best-fit IC_{50} and m varied widely across NAbs (Fig. 1b). IC_{50} values ranged from ~10^{-3} to ~140 μg ml^{-1} (Fig. 1b), in close agreement with reported estimates (Supplementary Fig. 3a and Supplementary Data 1). The values of m, the importance of which has been recognized with HIV-1 and hepatitis C[45,46] but has not typically been reported for SARS-CoV-2, ranged from ~0.2 to 2 (Fig. 1c). This variability in IC_{50} and m was not restricted to a particular pseudotyped virus construct or backbone (Supplementary Fig. 3b,c),

[1]Clem Jones Centre for Ageing Dementia Research, Queensland Brain Institute, The University of Queensland, Brisbane, Queensland, Australia. [2]Department of Chemical Engineering, Indian Institute of Science, Bangalore, India. [3]Centre for Biosystems Science and Engineering, Indian Institute of Science, Bangalore, India. [4]Present address: Certara QSP, Certara UK Limited, Sheffield, UK. ✉e-mail: p.padmanabhan@uq.edu.au; narendra@iisc.ac.in

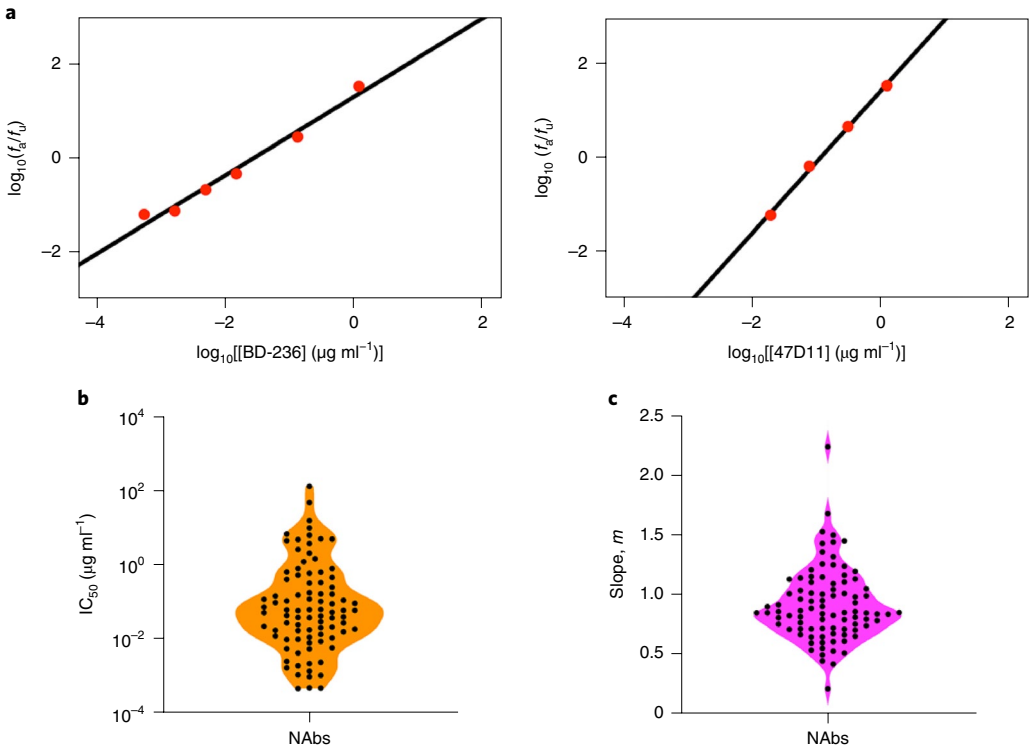

Fig. 1 | Analysis of the dose–response curves of SARS-CoV-2 NAbs. a, Fits (lines) of the median-effect equation to published experimental data (circles) of the fraction of infection events blocked (f_a) as a function of NAb concentration, shown for two NAbs, BD-236 (left) and 47D11 (right). Experimental data points with $1\% < f_a < 99\%$ (circles) were considered for parameter estimation. Fits for the remaining NAbs are provided in Supplementary Fig. 2. f_u and f_a are the fraction of infection events that are unaffected and affected respectively, by the NAbs in a single round of infection. **b**,**c**, The best-fit estimates of IC_{50} (**b**) and m (**c**) for all the NAbs analyzed (Supplementary Data 1).

cell line (Supplementary Fig. 3d,e) or assay conditions, which could vary across studies (Supplementary Fig. 3f,g). The variability was thus not attributable to these potential confounding factors and appeared to be intrinsic to the NAbs, indicating the spectrum of NAbs elicited. Furthermore, akin to HIV-1 antibodies[45], the variations in IC_{50} and m appeared independent. For example, the NAbs BD-361 and REGN10954 had similar IC_{50} values (both ~0.04 μg ml^{-1}) but vastly different m (~0.7 and ~1.5, respectively), whereas the NAbs CC12.3 and 515-5 had different IC_{50} values (~0.02 μg ml^{-1} and 1.6 μg ml^{-1}, respectively) but similar m (both ~1). IC_{50} and m were thus not only sufficient but also necessary for quantifying the neutralization efficiencies of NAbs. We therefore employed IC_{50} and m as the shape parameters. Plotting the NAbs on an IC_{50}–m plot, we identified the NAb shape space (Fig. 2), which, because of its two-dimensional nature, we termed the 'landscape of SARS-CoV-2 NAbs'.

The landscape contains potent NAbs, with low IC_{50} and high m, as well as weak NAbs, with the opposite traits. To compare the NAbs, we employed the instantaneous inhibitory potential (IIP), a composite metric of IC_{50} and m (refs. [45–47]). IIP_D represents the $\log_{10}$ decline in viral load in a single round infection assay due to the NAb present at concentration D. Thus, the higher the IIP_D, the more potent is the NAb at that concentration. NAbs displayed a wide distribution of IIP_{100} values: six NAbs had the highest IIP_{100} values, >5, and seven had the least, ≤1 ($D = 100$ μg ml^{-1}) (Fig. 2b and Supplementary Data 1). This distribution demonstrated further the wide spectrum of neutralization efficiencies of NAbs. Using another NAb concentration did not affect this distribution substantially (Supplementary Fig. 4).

Prediction of the NAb responses of convalescent patients. The landscape established bounds on the neutralization efficiencies of the NAbs elicited. We reasoned next that the diversity of the NAb responses across individuals would arise from the way NAbs are sampled from the landscape. Although a large number of NAbs can be isolated from individuals, studies of convalescent patient plasma[26,27,48–50] as well as on NAb epitope profiling[51] have argued that the NAb response of an individual can be attributed to a small subset of five to ten distinct NAbs. Furthermore, although some epitopes on the SARS-CoV-2 spike protein, S, are targeted more than others by NAbs, the collection of NAbs produced differs substantially across individuals[52]. We therefore assumed that the response elicited by an infected individual would be a small, random subset of the landscape. We analyzed DRCs of NAbs isolated from individual patients and found that they indeed constituted such subsets (Supplementary Fig. 5). Accordingly, we sampled random combinations of ten NAbs each, each combination representing the response of an individual. Our results were robust to an increase in the number of NAbs sampled beyond ten (Supplementary Fig. 6). We let NAb concentrations vary across individuals, to mimic the observed variation of the NAb titers[48–50]. We quantified the neutralization efficiency of the NAb response by simulating standard plasma dilution assays (Methods and Fig. 3a). Experimental plasma dilution assay results follow an inverse sigmoidal pattern and are characterized by NT_{50}, the dilution at which the neutralization efficiency of the plasma decreases by 50% (Fig. 3b). In our simulations, we let the NAbs exhibit Bliss independence or Loewe additivity, the former representing NAbs targeting distinct, non-occluding epitopes and the latter the same or occluding epitopes[53]. Our simulations recapitulated the dilution curves associated with patient plasma (Fig. 3b). Furthermore, the values of NT_{50} we predicted were in close agreement with experimental observations[49] (Fig. 3c). (Note that immunoglobulin-G (IgG) targeting the receptor binding domain of the

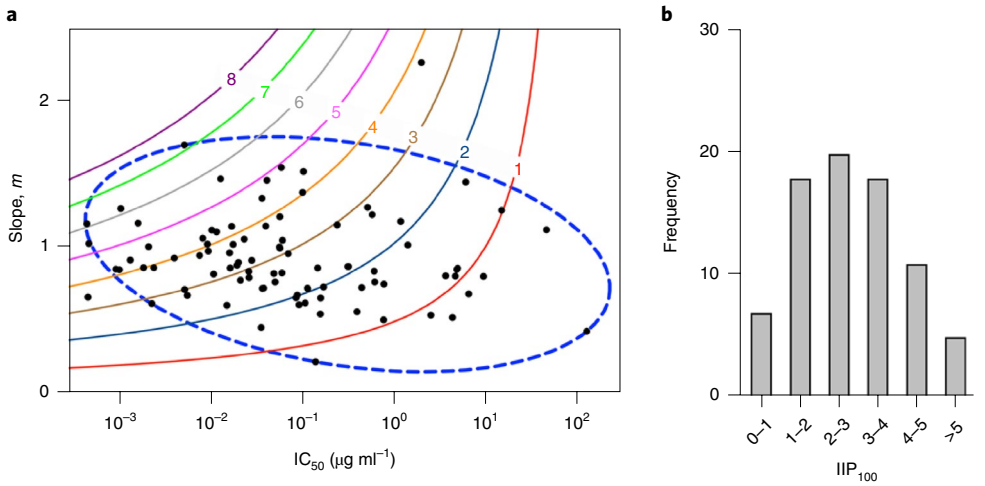

Fig. 2 | The landscape of SARS-CoV-2 NAbs. a, The SARS-CoV-2 NAbs analyzed in Fig. 1, depicted on an IC_{50}–*m* plot. Each dot represents a NAb. Nine NAbs that have multiple neutralization curves reported are represented multiple times (Supplementary Data 1). Solid lines are loci of points corresponding to fixed IIP values computed at 100 μg ml^{-1}. The ellipse (blue dashed line) circumscribes the landscape of SARS-CoV-2 NAbs elicited. **b**, The distribution of IIP_{100} values of the NAbs. Average IIP_{100} values are used for the nine NAbs for which multiple curves are reported.

SARS-CoV-2 spike protein, reported in the experiments in Fig. 3c, do not represent all NAbs. They are, however, a major component of the NAbs. The dilution assays in Fig. 3b do include all NAbs, indicating that our predictions capture the measured NT_{50} values reliably.) The latter data were described better by Bliss independence at low NAb titers and Loewe additivity at high titers. This is expected, because, at low titers, the NAbs are unlikely to interact with each other and would thus follow Bliss independence, whereas at high titers, they may compete for binding sites on S or occlude each other and exhibit Loewe additivity[53]. At any NAb titer, there existed substantial variation in NT_{50}, attributed to the random combinations of NAbs sampled. The variation, however, was outweighed by the overall rise of NT_{50} with the NAb titer, consistent with patient data (Fig. 3c). For example, the geometric mean NT_{50} computed using Loewe additivity was 7.2 at an IgG titer of 0.1 μg ml^{-1} and 455.1 at 10 μg ml^{-1}. Sampling from the NAb landscape thus successfully recapitulated patient responses. Note that no adjustable parameters were involved in this comparison. We were thus able to describe the diversity of the NAb responses elicited across patients. Armed with this description, we examined next the protection accorded by vaccines in clinical trials.

Prediction of COVID-19 vaccine efficacies. Following vaccination, NAb titers rise and are expected to remain stable (or decay slowly) over weeks to months[54], protecting individuals exposed to the virus during this period. Individuals were assumed to be protected if they did not report symptomatic infection. Loss of protection involved symptoms and a positive result on a nucleic acid amplification test[10,11]. Protection with NAbs is not expected to be sterilizing, as suggested by animal studies[21,55]; NAbs help suppress virus load and facilitate more rapid clearance of the infection. We assumed that the severity of the symptoms would be proportional to the virus load. If the peak is sufficiently suppressed, no symptoms may result, as is the case with naturally asymptomatic infections[56]. Here we assumed that an individual would be detected as symptomatically infected if the viral load rose above a threshold.

To estimate the peak viral load, we developed a mathematical model (Fig. 4a) of the early time course of the infection, where the viral load typically rises, attains a peak and declines[57]. To ascertain its ability to describe these dynamics in vivo, we fit the model to longitudinal viral load data from individual patients from three cohorts[57–59]. The model fit the data well (Fig. 4b and Supplementary Figs. 7 and 8) and yielded parameter estimates quantifying inter-patient variability in the within-host dynamics (Supplementary Tables 2 and 3). We applied the model to describe the effect of vaccination (Methods). We assumed that NAbs generated following vaccination would exist at the start of infection. Although NAbs may perform many functions, including stimulating the cellular adaptive response[56,60], direct evidence of these functions in SARS-CoV-2-infected humans is yet to be gathered[56]. (The vaccines may stimulate other immune arms independently of the NAbs, which, as we argue above, is expected to make limited contributions to vaccine efficacy against the wild-type SARS-CoV-2 strain[10,11,17,18].) We therefore focused on their ability to neutralize free viruses, effectively reducing viral infectivity. We recall that protection due to NAbs is not expected to be sterilizing[21,55]. The reduced infectivity is also consistent with in vitro pseudovirus neutralization assays, which measure the drop in infectivity with increasing NAb concentrations. Our model captures these in vitro assays quantitatively (Fig. 3). The greater the reduction in infectivity, the lower the peak viral load in vivo (Fig. 4c, curves with efficacy $\varepsilon > 0$). This assumption of the activity of NAbs is thus also consistent with the inverse correlation between the peak viral load and NAb titers elicited by vaccination in mouse models[21] and in macaques[61].

Substantial de novo NAb production post-infection typically occurs after the peak in virus load[56] and has been argued to have limited impact on viral clearance[62]. We therefore considered pre-existing NAbs as responsible for protection and assumed their titers not to vary substantially during the course of the infection, given the typically short course of the infection and the much longer durability of the NAb response to vaccination[54]. We let the pre-existing NAbs be drawn as random subsets from the landscape, as we did above. We assumed that the NAbs neutralized free viruses with an efficiency that we estimated using Loewe additivity. NAb titers in the lung airways are expected to be similar to those in the blood given the close coupling between the lungs and the circulatory system[56]. The efficiency of NAbs in vivo can differ from that in vitro[63], which we took into account. We simulated a virtual patient population of 3,500 individuals, similar to the number of individuals infected in the placebo arms of clinical trials. The individuals all had distinct viral dynamics parameters drawn from previously known and/or estimated ranges (Supplementary Tables 1 and 2), to mimic inter-patient variability in addition to the variability arising from NAb sampling from the landscape. Our model predicted wide variability

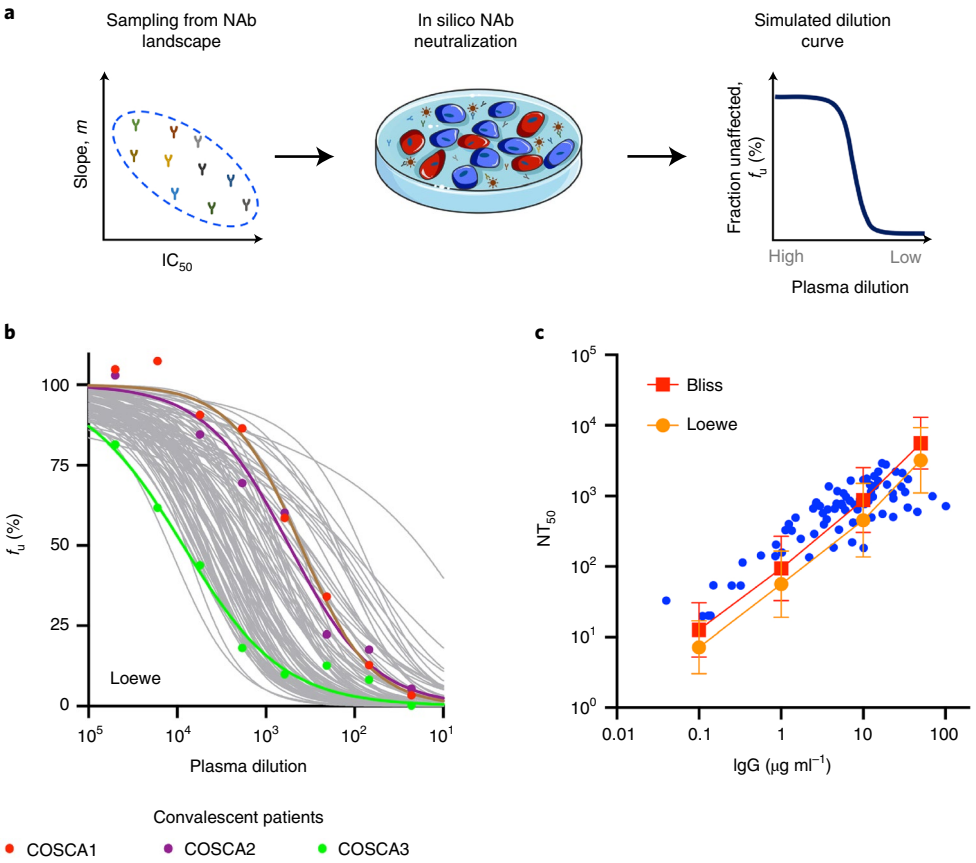

Fig. 3 | NAb landscape and patient responses. a, Schematic of the procedure to predict plasma dilution curves. **b**, Predictions (gray lines) of plasma dilution curves. Each line represents a patient. We assumed ten NAbs per patient and $D_0 = 30\,\mu g\,ml^{-1}$. Also shown are plasma dilution assays from three patients[82]. Patient IDs are indicated alongside the symbols used. The measurements (colored symbols) followed $f_u = \frac{(\gamma)^n}{(\gamma)^n + (NT_{50})^n}$ (lines), where n is the Hill coefficient, γ is the plasma dilution and NT_{50} is the half-maximal inhibitory plasma neutralizing titer. **c**, Half-maximal inhibitory plasma neutralizing titers, NT_{50}, as a function of total NAb concentration. Blue circles are reported estimates of IgG levels targeting the SARS-CoV-2 S receptor binding domain in convalescent patients. Red squares and orange circles are the geometric means of NT_{50} values predicted from 100 virtual patients at each NAb concentration using Bliss independence and Loewe additivity, respectively. The error bars are geometric standard deviations.

in the peak viral load (Fig. 4d). At low pre-existing NAb concentrations ($0.01\,\mu g\,ml^{-1}$), indicative of the scenario without vaccination, the predicted peak viral load ranged from ~10^3 to 10^9 copies per milliliter, consistent with the range in symptomatic individuals[64]. The peaks declined as NAb titers increased. Following clinical trials, we set the limit of detection to ~10^2 copies per milliliter (ref. [65]). (Note that, even if symptoms were to arise with lower viral loads in some individuals, such individuals would not be diagnosed as infected because of assay limitations.) The fraction of individuals with peaks below detection would indicate the level of protection due to the vaccine.

To quantify the mean level of protection and test it against data from clinical trials, we used viral dynamics parameters representative of detectable infections[66,67] (Supplementary Tables 1 and 2) and simulated the dynamics in a cohort of 10,000 infected individuals. Vaccination studies report the NT_{50} values of the NAb responses elicited and the associated mean protection level, or efficacy[7,10,12,68–70] (Supplementary Table 4). We binned individuals into narrow NT_{50} bands and calculated the mean protection and 95% confidence interval (CI) in each band. We found that the mean protection was low for an NT_{50} of ~1. It increased in a sigmoidal manner to 50% at an NT_{50} of ~15 and asymptotically reached 100% at an NT_{50} of ~200 (Supplementary Fig. 9).

To compare these predictions with clinical data across trials, we normalized the data using the NT_{50} values from convalescent patients reported by the respective trials (Supplementary Table 4). This ensured that assay variations across studies did not confound our comparisons. We accordingly also normalized our predictions of NT_{50} with those corresponding to convalescent patients captured by our model (Methods, Fig. 3 and Supplementary Fig. 10). For the set of parameters employed, the data for all the eight approved vaccines we considered fell on this 'protection curve' (Fig. 5). Thus, for example, a single dose of the vaccine Ad26.COV2.S elicited NAbs with a scaled NT_{50} of 0.43 and accorded 66.1% protection. Following two doses of the vaccine BNT162b2, the corresponding values were 3.84% and 94%, respectively. These values were captured accurately by our model predictions. This agreement extended to data from phase III trials of the other vaccines we considered as well (Fig. 5).

We tested the robustness of these predictions to model parameter variations. Using local (Supplementary Fig. 11a) and global sensitivity analysis (Supplementary Fig. 11b), we found that our predictions of vaccine efficacy were robust to parameter variations so long as the parameter values were consistent with patient data (Supplementary Fig. 11c–e). One parameter not involved in the patient data fitting was ω, the assumed ratio of the IC_{50} values of the NAbs in vivo and in vitro, because NAb responses, given their limited role, were not part of our model of unvaccinated individuals[62]. The protection curve was sensitive to ω (Supplementary Fig. 11f). Recent studies[71,72] have estimated ω for a few NAbs of SARS-CoV-2 and found it to be in the range ~5–40 (Supplementary Table 1), similar

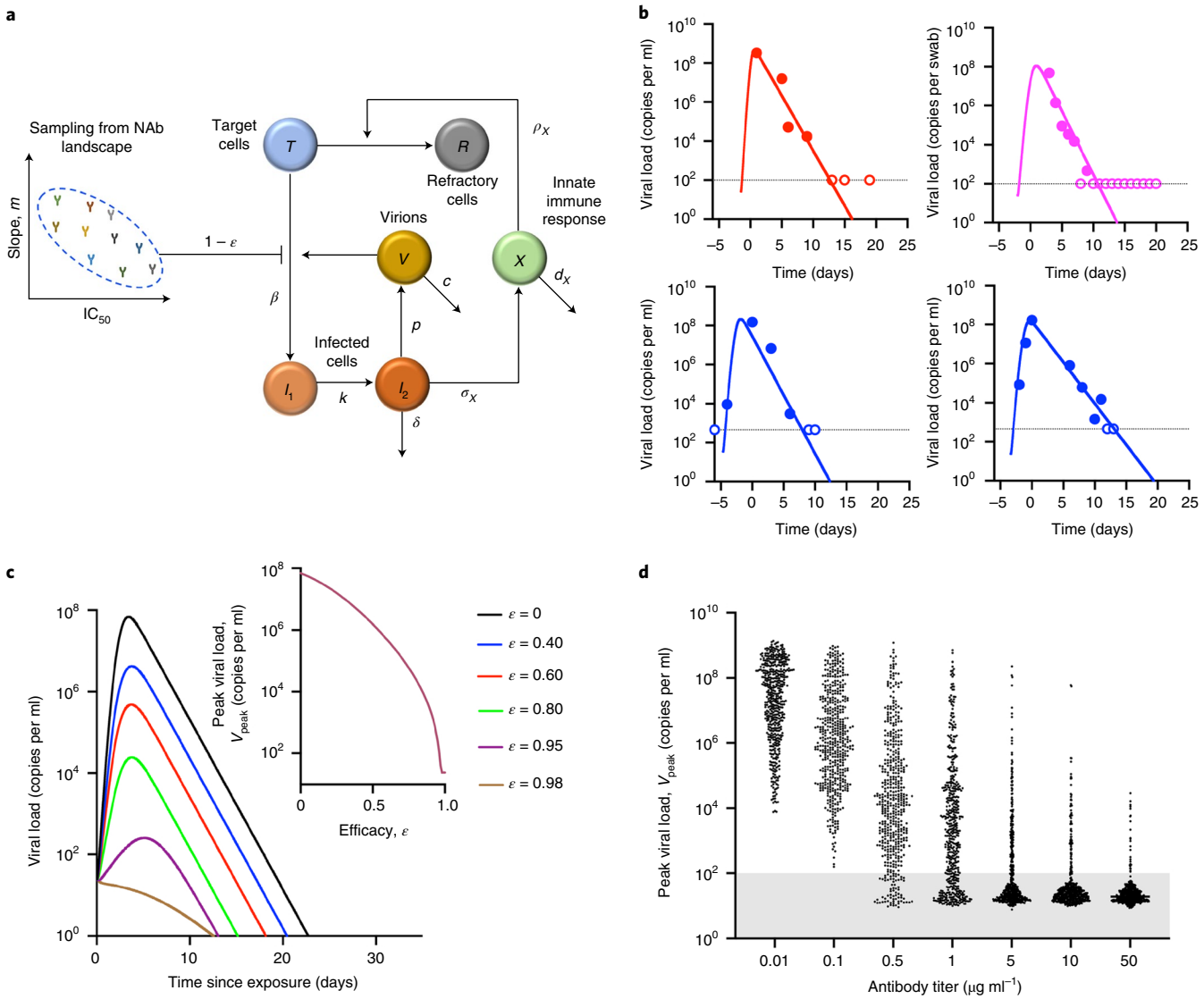

Fig. 4 | Modeling SARS-CoV-2 dynamics and the effect of vaccination. a, Schematic of the model of within-host SARS-CoV-2 dynamics depicting the interactions between target cells *T*, infected cells I_1 and I_2, refractory cells *R*, virions *V*, innate immune response *X* and pre-existing NAbs, sampled from the landscape. **b**, Representative fits of model predictions of viral load observed in non-vaccinated French[58] (red), US[59] (blue) and German[57] (magenta) cohorts. Fits to data from all the patients studied are shown in Supplementary Fig. 7. The grey horizontal lines indicate the limit of detection. **c**, Predictions of viral load in non-vaccinated (black line) and vaccinated (colored lines) individuals with different fixed efficacies of the NAbs indicated. Inset: predicted peak viral load at different efficacies. **d**, Predictions of peak viral load at different NAb titers. Each dot represents a patient. The grey region contains peak viral loads below the detection limit.

to estimates for other viruses[63,73]. In the above predictions we set ω to ~10, which lies in the above range and yielded the protection curve that captured clinical data. Future studies may provide independent estimates of the model parameters, limiting these uncertainties and sharpening the mechanistic links between COVID-19 vaccine efficacies and NAb responses assumed in our formalism.

Discussion

Our formalism for predicting COVID-19 vaccine efficacies as a function of the NAb responses they elicit required the description and integration of several key phenomena, varying over many length and time scales. These include (1) the neutralization potential of individual NAbs, (2) the diversity of the NAb response within and across individuals, (3) the relationship between NAb titers in individuals and their neutralization potential, (4) the within-host dynamics of disease progression, (5) the influence of vaccination on the within-host dynamics and (6) the variability of the latter influence across a patient population in clinical trials. At each step, we established quantitative connects with experimental data, rendering our approach rigorous.

Identifying correlates of the protection offered by COVID-19 vaccines has been challenging[74]. Several recent studies have pointed to NAb responses as strong correlates of vaccine-mediated protection[17–20]. Our study independently arrived at the correlation between vaccine efficacy and NT_{50} and generated testable hypotheses of its mechanistic origins. Briefly, our study assumed that, in response to vaccination, different individuals in a population produce NAbs that are well represented by random samples from the NAb landscape. The neutralization potential of the NAbs elicited, quantified by NT_{50}, accordingly varies across individuals in a dose-dependent manner. The presence of the NAbs, in our model, caused a reduction in the peak viral load following infection, also in a dose-dependent

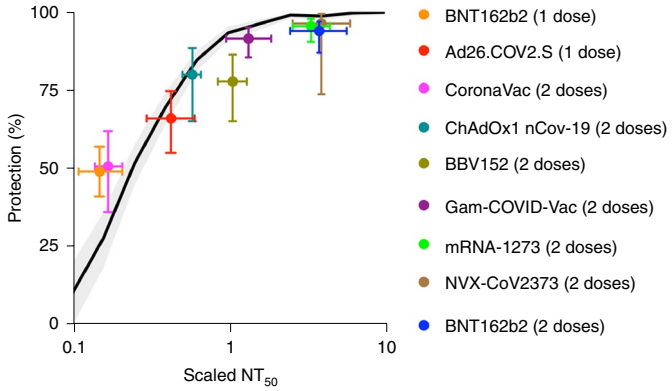

Fig. 5 | Protection post vaccination. Model predictions of the relationship between vaccine efficacy and NT_{50} (solid line) compared with data from vaccination trials (symbols). The number of doses of the vaccine administered is indicated in parentheses. The error bars and the shaded region represent the 95% confidence intervals. The data from the trials used are summarized in Supplementary Table 5. The model equations and simulation procedure are described in Methods.

manner. A sufficient reduction in the peak viral load was assumed to prevent symptoms and manifest as protection conferred by vaccination, potentially giving rise to the correlation of vaccine efficacy with NT_{50}. Thus, our study suggests a plausible mechanism that can be tested experimentally for how multiple NAbs generated within an individual following vaccination provide protection by being members of a shape space. Our model proposes a mechanism to reduce the net neutralization effect of these antibodies into a single metric. Further, our formalism deduced a relationship between NT_{50} and the concentration of NAbs in plasma, so that the latter may also be used to estimate vaccine efficacies.

Our formalism employs several assumptions and hypotheses underlying the protection conferred by NAbs elicited by vaccination. First, NAbs are assumed to be generated randomly from the NAb landscape. Although this appears plausible (Supplementary Fig. 5), it remains to be established. Furthermore, that the NAb landscape in convalescent patients and following vaccination is similar needs to be ascertained. Second, assay variations in the estimates of NAb characteristics (IC_{50} and m) are assumed not significant. To verify this, estimates of IC_{50} and m could be standardized across studies, for example, by normalizing them using the IC_{50} and m values generated in each study for the same 'reference' NAb and by using the same viral backbone and cell line. Third, our model assumed that protection following vaccination is predominantly due to NAbs and that other immune arms play a secondary role. Although the extent to which COVID-19 vaccines trigger other immune arms is being investigated[20], the high NAb titers generated after the boost support this assumption. Fourth, NAbs are assumed to act primarily by neutralizing virus and thus reducing viral infectivity and the peak viral load in a dose-dependent manner. It is possible that NAbs trigger other immune arms, via Fc-mediated mechanisms[20]. Innate immune responses and CD8 T cells may also reduce the peak viral load[56,75]. The contributions of these mechanisms to vaccine efficacy remain to be ascertained. Fifth, the severity of symptoms is assumed to depend on the viral load. In clinical trials of vaccine efficacy, individuals are diagnosed after symptom onset. If the minimum viral load for symptom onset, which is unknown, is greater than the assay limit of 100 copies per milliliter, fewer people would display symptoms than would test positive on a nucleic acid test if all individuals were frequently monitored. Vaccine efficacy trials thus report protection against symptoms, whereas our model predicts protection against positivity in a nucleic acid test. The latter might be slightly lower than the former. Sixth, our within-host model assumes that innate immune responses would render target cells refractory to infection. Although this has been observed with other viruses[76], and has been used in models of SARS-CoV-2 dynamics[77], it remains to be demonstrated explicitly in vivo. Seventh, although we assessed the robustness of our model to parameter variations, several of the parameter values employed were based on previous studies or from other viral infection settings. For example, we assumed that the ratio of the neutralization efficiency of NAbs in vitro and in vivo, ω, was a constant. We set its value, based on estimates for a few NAbs, to one that helped recapitulate clinical data. However, ω might vary across NAbs. Knowledge of these parameter values would make our model more robust and improve its predictive ability. Challenge studies on macaques post vaccination could help test these assumptions.

Finally, we note that our study did not consider viral mutations. With five to ten NAbs active, viral escape from NAb responses is expected to be unlikely[51,78]. With the new circulating mutant strains[7], however, the NAb landscape may have to be reconstructed. Future studies may report DRCs of NAbs against the new strains, facilitating such reconstruction. Our formalism could then be applied to predict the efficacies of vaccines against the new strains.

Methods

Data of DRCs. We considered data from studies that reported in vitro DRCs of NAbs using SARS-CoV-2 pseudotyped virions[26,27,30–32,34–44]. We included early studies in our analysis so that the NAbs considered were unlikely to be against mutant virus strains. The assays estimated the fraction of infection events unaffected by the NAbs as a function of the NAb concentration (Fig. 1 and Supplementary Fig. 2). We extracted the data using Engauge Digitizer 12.1 and ensured consistency with reported details, such as dilution levels used.

Analysis of DRCs. We used the median-effect equation (equation (1)) to analyze the data:

$$\log_{10}\left(\frac{f_a}{f_u}\right) = m\log_{10}\left(\frac{D}{IC_{50}}\right) \quad (1)$$

where f_u and f_a are the fraction of infection events unaffected and affected, respectively, by the NAbs in a single round of infection, D is the NAb concentration, IC_{50} is the half-maximal inhibitory concentration and m is the slope. Data were fitted using the tool REGRESS in MATLAB R2017b. Data points with $1\% < f_u < 99\%$ were considered for parameter estimation. We fit the data using equation (1), with m and $-m\log_{10}(IC_{50})$ as adjustable parameters, and obtained estimates of IC_{50} and m for each NAb. We then computed $IIP_{100} = \log_{10}\left(1 + \left(\frac{100}{IC_{50}}\right)^m\right)$. We did not include NAbs for which the fits were not satisfactory ($R^2 \leq 0.8$; Supplementary Data 1), possibly arising from large uncertainties in the data. The details of the NAbs and parameter estimates are presented in Supplementary Data 1.

In silico simulation of plasma dilution assays. We simulated plasma dilution experiments as follows. We assumed that the plasma contained N NAbs in equimolar concentrations sampled from the landscape (Fig. 2a). The reciprocal plasma dilution curve was predicted assuming Loewe additivity (equation (2)) or Bliss independence (equation (3)) between the different NAbs[79–81] using

$$\sum_{i=1}^{N} \frac{D_i/\gamma}{IC_{50_i}\left(\frac{1}{\varepsilon_L} - 1\right)^{-1/m_i}} = 1 \quad (2)$$

$$\varepsilon_B = 1 - \prod_{i=1}^{N} \frac{(IC_{50_i})^{m_i}}{(IC_{50_i})^{m_i} + (D_i/\gamma)^{m_i}} \quad (3)$$

where γ is the plasma dilution factor, ε_L and ε_B are the fractions of infection events affected by the plasma in a single round of infection estimated using Loewe additivity and Bliss independence, respectively, D_i is the concentration of the ith NAb in the plasma before dilution, and IC_{50} is its half-maximal inhibitory concentration and m_i its slope, with $i \in \{1, 2, \ldots, N\}$. We let $N = 10$ in our simulations[26]. We estimated the value of γ at which $\varepsilon = 0.5$ as the corresponding NT_{50}. We chose D_i as D_0/N, and varied D_0 between 0.1 and 100 μg ml^{-1} (D_0 is the total NAb concentration).

We repeated these simulations 100 times at different NAb titers, with each simulation representative of an individual patient. We compared the resulting predictions at $D_0 = 30$ μg ml^{-1} with observations from three patients (Fig. 3b)[82], which we also digitized. The equation $f_u = \frac{(\gamma)^n}{(\gamma)^n + (NT_{50})^n}$ was fit to the observations from three patients, merely to ascertain the shapes of the curves and their

similarity to those predicted by our calculations. Here, n is the Hill coefficient, γ is the plasma dilution and NT_{50} is the half-maximal inhibitory plasma neutralizing titer. We also compared predictions of the dependence of NT_{50} on NAb titers with experimental observations (Fig. 3c)[49].

Model of SARS-CoV-2 dynamics. To predict the protection conferred by vaccines, we developed a mathematical model of within-host SARS-CoV-2 infection post vaccination. We adapted previous models[58,67,77,83] by focusing on early dynamics, required to accurately predict the reduction in the peak viral load due to pre-existing NAbs. The following equations described the resulting infection dynamics in vaccinated individuals exposed to the virus:

$$\frac{dT}{dt} = -\beta(1-\varepsilon)VT - \rho_X XT \tag{4}$$

$$\frac{dR}{dt} = \rho_X XT \tag{5}$$

$$\frac{dI_1}{dt} = \beta(1-\varepsilon)VT - kI_1 \tag{6}$$

$$\frac{dI_2}{dt} = kI_1 - \delta I_2 \tag{7}$$

$$\frac{dV}{dt} = pI_2 - cV \tag{8}$$

$$\frac{dX}{dt} = \frac{\sigma_X I_2(1-X)}{\phi_X + I_2} - d_X X \tag{9}$$

Here, uninfected target cells, T, are infected by SARS-CoV-2 virions, V, with second-order rate constant β, producing infected cells in eclipse phase, I_1. Cells I_1 convert to productively infected cells, I_2, with a rate constant k. Cells I_2 produce virions at rate p per cell and are lost with rate constant δ. This transition from target cells to infected cells in the eclipse phase and then the productive phase has been employed in previous models[58,77]. The virions are cleared with rate constant c. The activation of the innate immune response, quantified phenomenologically using X, is assumed to be a saturable function of I_2, with maximal rate σ_X and half-maximal activation parameter ϕ_X. If I_2 is not limiting, X would rise at rate σ_X at low X and cease to rise as X approaches 1. This form for the innate immune response has been proposed previously[84]. X converts uninfected cells to an infection-refractory state, R, at a per capita rate ρ_X, and decays with rate constant d_X. The presence of the refractory population has also been proposed in previous models[77,85,86]. The pre-existing NAbs are drawn as random subsets from the landscape (Fig. 2a) to block new infections with an efficacy ε, which is a function of NAb titers and computed using

$$\sum_{i=1}^{N} \frac{D_i/\gamma}{\omega IC_{50_i}\left(\frac{1}{\varepsilon}-1\right)^{-1/m_i}} = 1$$

where ω accounts for the difference between in vitro and in vivo IC_{50} values[63,71]. The neutralizing activity of NAbs follows from our observations above (Fig. 3), where this activity recapitulated plasma dilution experiments.

Fits to longitudinal patient data. We considered viral load data from non-vaccinated individuals in three cohorts. One dataset[57] has patients with mild symptoms. The second dataset[59] has measurements in the viral expansion phase. We chose nine individuals from the latter dataset who had frequent viral load measurements. The third dataset[58] has data from hospitalized patients classified by their age (above and below 65 years). We simultaneously fit our viral dynamics model (equations (4)–(9)) to viral loads from all three datasets using a population-based fitting approach via nonlinear mixed effects models (Supplementary Section 1).

Prediction of vaccine efficacy. *Vaccine efficacy.* To examine the variation in peak viral loads with NAb titers (Fig. 4d), we predicted the viral dynamics of 3,500 infected individuals, each individual with different pre-existing NAbs sampled from the landscape as well as different values of viral dynamics parameters (Supplementary Tables 1 and 2). To obtain the protection curve (Fig. 5), we sampled antibody concentrations from a uniform distribution ranging between 0.05 and 100 $\mu g\,ml^{-1}$, mimicking the range seen experimentally, and simulated viral dynamics in 10,000 virtual individuals, as we describe above, and obtained peak viral loads. Furthermore, for each individual, we also simulated plasma dilution assays and estimated NT_{50}. We then binned individuals into narrow ranges of NT_{50} values. In each bin, we estimated the fraction of individuals with peak viral load below 100 copies per milliliter. This fraction yielded the protection curve. The error bars (95% CI) were obtained using the Clopper–Pearson method and following the protocols used in clinical trials[10,87,88].

Convalescent NT_{50}. Our model captured the experimentally observed dependence of NT_{50} on NAb titers in 15 convalescent patients (Fig. 3c)[49]. NT_{50} as a function of time post symptom onset has also been measured in the study described in ref. [49]. Following vaccine immunogenicity studies[28,89], we randomly sampled one timepoint per patient at least 20 days after initial symptoms and obtained a geometric mean NT_{50} of 565 (Supplementary Fig. 10). We used this value to normalize the NT_{50} predicted by our model.

Parameter sensitivity. The available longitudinal patient data did not allow estimation of all the parameters in our model. We thus fixed several parameters (ρ_X, σ_X, Φ_X, k, c and d_X) and initial conditions ($T(0)$ and $I_2(0)$) to values from previous studies and estimated the rest (β, p and δ) from fits to patient data (Methods). Overall, the good fits (Fig. 4b and Supplementary Fig. 7) indicate that the parameters recapitulate the patient viral load data. Yet, the choice of values of the 'fixed' parameters could introduce uncertainties in the overall parameter estimates. We therefore tested the sensitivity of model predictions of vaccine efficacy to fixed model parameter values and initial conditions by increasing or decreasing the parameter values by twofold, one at a time (Supplementary Fig. 11a). We also performed a global sensitivity analysis and estimated the partial rank correlation coefficients of each parameter (Supplementary Fig. 11b). We found that the vaccine efficacy predictions were most sensitive to the viral clearance rate, c. We therefore varied c, refitted the model to patient data using the same adjustable parameters, and repeated our vaccine efficacy predictions. The protection curves were close to the one described above (Supplementary Fig. 11c). We also obtained protection curves using two different iterations after fitting using Monolix (Supplementary Fig. 11d) and when fixed parameter values were varied over a defined range or held constant (Supplementary Fig. 11e). Finally, we tested the sensitivity of the protection curve to the IC_{50} values of the NAbs in vivo by varying ω (Supplementary Fig. 11f).

Data availability

All data supporting the findings of this study are available within the paper and its Supplementary Information files. Source data are provided with this paper.

Code availability

The codes are written in MATLAB and are available on GitHub (https://github.com/PraneshPadmanabhan/COVID-19-vaccine-efficacies) and on Zenodo[90].

Received: 27 April 2021; Accepted: 20 January 2022;
Published online: 28 February 2022

References

1. Wouters, O. J. et al. Challenges in ensuring global access to COVID-19 vaccines: production, affordability, allocation and deployment. *Lancet* **397**, 1023–1034 (2021).
2. Forni, G. & Mantovani, A. COVID-19 vaccines: where we stand and challenges ahead. *Cell Death Differ.* **28**, 626–639 (2021).
3. Shrotri, M., Swinnen, T., Kampmann, B. & Parker, E. P. K. An interactive website tracking COVID-19 vaccine development. *Lancet Glob. Health* **9**, e590–e592 (2021).
4. Koup, R. A. et al. A government-led effort to identify correlates of protection for COVID-19 vaccines. *Nat. Med.* **27**, 1493–1494 (2021).
5. Saad-Roy, C. M. et al. Epidemiological and evolutionary considerations of SARS-CoV-2 vaccine dosing regimes. *Science* **372**, 363–370 (2021).
6. Bubar, K. M. et al. Model-informed COVID-19 vaccine prioritization strategies by age and serostatus. *Science* **371**, 916–921 (2021).
7. Voysey, M. et al. Single-dose administration and the influence of the timing of the booster dose on immunogenicity and efficacy of ChAdOx1 nCoV-19 (AZD1222) vaccine: a pooled analysis of four randomised trials. *Lancet* **397**, 881–891 (2021).
8. Garg, A. K., Mittal, S., Padmanabhan, P., Desikan, R. & Dixit, N. M. Increased B cell selection stringency in germinal centers can explain improved COVID-19 vaccine efficacies with low dose prime or delayed boost. *Front. Immunol.* **12**, 776933 (2021).
9. Tauzin, A. et al. Strong humoral immune responses against SARS-CoV-2 spike after BNT162b2 mRNA vaccination with a 16-week interval between doses. *Cell Host Microbe* **30**, 97–109 (2022).
10. Baden, L. R. et al. Efficacy and safety of the mRNA-1273 SARS-CoV-2 vaccine. *N. Engl. J. Med.* **384**, 403–416 (2021).
11. Polack, F. P. et al. Safety and efficacy of the BNT162b2 mRNA COVID-19 Vaccine. *N. Engl. J. Med.* **383**, 2603–2615 (2020).
12. Logunov, D. Y. et al. Safety and efficacy of an rAd26 and rAd5 vector-based heterologous prime-boost COVID-19 vaccine: an interim analysis of a randomised controlled phase 3 trial in Russia. *Lancet* **397**, 671–681 (2021).

13. Ella, R. et al. Efficacy, safety, and lot-to-lot immunogenicity of an inactivated SARS-CoV-2 vaccine (BBV152): interim results of a randomised, double-blind, controlled, phase 3 trial. *Lancet* **398**, 2173–2184 (2021).
14. Jara, A. et al. Effectiveness of an inactivated SARS-CoV-2 vaccine in Chile. *N. Engl. J. Med.* **385**, 875–884 (2021).
15. Sadoff, J. et al. Safety and efficacy of single-dose Ad26.COV2.S vaccine against COVID-19. *N. Engl. J. Med.* **384**, 2187–2201 (2021).
16. Heath, P. T. et al. Safety and efficacy of NVX-CoV2373 COVID-19 vaccine. *N. Engl. J. Med.* **385**, 1172–1183 (2021).
17. Khoury, D. S. et al. Neutralizing antibody levels are highly predictive of immune protection from symptomatic SARS-CoV-2 infection. *Nat. Med.* **27**, 1205–1211 (2021).
18. Earle, K. A. et al. Evidence for antibody as a protective correlate for COVID-19 vaccines. *Vaccine* **39**, 4423–4428 (2021).
19. Feng, S. et al. Correlates of protection against symptomatic and asymptomatic SARS-CoV-2 infection. *Nat. Med.* **27**, 2032–2040 (2021).
20. Barrett, J. R. et al. Phase 1/2 trial of SARS-CoV-2 vaccine ChAdOx1 nCoV-19 with a booster dose induces multifunctional antibody responses. *Nat. Med.* **27**, 279–288 (2021).
21. Israelow, B. et al. Adaptive immune determinants of viral clearance and protection in mouse models of SARS-CoV-2. *Sci. Immunol.* **6**, eabl4509 (2021).
22. Gilbert, P. B. et al. Immune correlates analysis of the mRNA-1273 COVID-19 vaccine efficacy clinical trial. *Science* **375**, 43–50 (2022).
23. Addetia, A. et al. Neutralizing antibodies correlate with protection from SARS-CoV-2 in humans during a fishery vessel outbreak with a high attack rate. *J. Clin. Microbiol.* **58**, e02107–e02120 (2020).
24. Lumley, S. F. et al. Antibody status and incidence of SARS-CoV-2 infection in health care workers. *N. Engl. J. Med.* **384**, 533–540 (2020).
25. Callow, K. A. Effect of specific humoral immunity and some non-specific factors on resistance of volunteers to respiratory coronavirus infection. *J. Hyg.* **95**, 173–189 (1985).
26. Liu, L. et al. Potent neutralizing antibodies against multiple epitopes on SARS-CoV-2 spike. *Nature* **584**, 450–456 (2020).
27. Robbiani, D. F. et al. Convergent antibody responses to SARS-CoV-2 in convalescent individuals. *Nature* **584**, 437–442 (2020).
28. Folegatti, P. M. et al. Safety and immunogenicity of the ChAdOx1 nCoV-19 vaccine against SARS-CoV-2: a preliminary report of a phase 1/2, single-blind, randomised controlled trial. *Lancet* **396**, 467–478 (2020).
29. Perelson, A. S. & Oster, G. F. Theoretical studies of clonal selection: minimal antibody repertoire size and reliability of self-non-self discrimination. *J. Theor. Biol.* **81**, 645–670 (1979).
30. Chi, X. et al. A neutralizing human antibody binds to the N-terminal domain of the Spike protein of SARS-CoV-2. *Science* **369**, 650–655 (2020).
31. Wang, C. et al. A human monoclonal antibody blocking SARS-CoV-2 infection. *Nat. Commun.* **11**, 2251 (2020).
32. Seydoux, E. et al. Analysis of a SARS-CoV-2-infected individual reveals development of potent neutralizing antibodies with limited somatic mutation. *Immunity* **53**, 98–105 e105 (2020).
33. Shi, R. et al. A human neutralizing antibody targets the receptor-binding site of SARS-CoV-2. *Nature* **584**, 120–124 (2020).
34. Wec, A. Z. et al. Broad neutralization of SARS-related viruses by human monoclonal antibodies. *Science* **369**, 731–736 (2020).
35. Lei, C. et al. Neutralization of SARS-CoV-2 spike pseudotyped virus by recombinant ACE2-Ig. *Nat. Commun.* **11**, 2070 (2020).
36. Lv, Z. et al. Structural basis for neutralization of SARS-CoV-2 and SARS-CoV by a potent therapeutic antibody. *Science* **369**, 1505–1509 (2020).
37. Zost, S. J. et al. Potently neutralizing and protective human antibodies against SARS-CoV-2. *Nature* **584**, 443–449 (2020).
38. Ju, B. et al. Human neutralizing antibodies elicited by SARS-CoV-2 infection. *Nature* **584**, 115–119 (2020).
39. Cao, Y. et al. Potent neutralizing antibodies against SARS-CoV-2 identified by high-throughput single-cell sequencing of convalescent patients' B cells. *Cell* **182**, 73–84 (2020).
40. Hansen, J. et al. Studies in humanized mice and convalescent humans yield a SARS-CoV-2 antibody cocktail. *Science* **369**, 1010–1014 (2020).
41. Rogers, T. F. et al. Isolation of potent SARS-CoV-2 neutralizing antibodies and protection from disease in a small animal model. *Science* **369**, 956–963 (2020).
42. Barnes, C. O. et al. Structures of human antibodies bound to SARS-CoV-2 spike reveal common epitopes and recurrent features of antibodies. *Cell* **182**, 828–842 (2020).
43. Pinto, D. et al. Cross-neutralization of SARS-CoV-2 by a human monoclonal SARS-CoV antibody. *Nature* **583**, 290–295 (2020).
44. Hanke, L. et al. An alpaca nanobody neutralizes SARS-CoV-2 by blocking receptor interaction. *Nat. Commun.* **11**, 4420 (2020).
45. Webb, N. E., Montefiori, D. C. & Lee, B. Dose–response curve slope helps predict therapeutic potency and breadth of HIV broadly neutralizing antibodies. *Nat. Commun.* **6**, 8443 (2015).
46. Padmanabhan, P. & Dixit, N. M. Inhibitors of hepatitis C virus entry may be potent ingredients of optimal drug combinations. *Proc. Natl Acad. Sci. USA* **114**, E4524–E4526 (2017).
47. Jilek, B. L. et al. A quantitative basis for antiretroviral therapy for HIV-1 infection. *Nat. Med.* **18**, 446–451 (2012).
48. Isho, B. et al. Persistence of serum and saliva antibody responses to SARS-CoV-2 spike antigens in COVID-19 patients. *Sci. Immunol.* **5**, eabe5511 (2020).
49. Iyer, A. S. et al. Persistence and decay of human antibody responses to the receptor binding domain of SARS-CoV-2 spike protein in COVID-19 patients. *Sci. Immunol.* **5**, eabe0367 (2020).
50. Röltgen, K. et al. Defining the features and duration of antibody responses to SARS-CoV-2 infection associated with disease severity and outcome. *Sci. Immunol.* **5**, eabe0240 (2020).
51. Shrock, E. et al. Viral epitope profiling of COVID-19 patients reveals cross-reactivity and correlates of severity. *Science* **370**, eabd4250 (2020).
52. Yuan, M. et al. Structural basis of a shared antibody response to SARS-CoV-2. *Science* **369**, 1119–1123 (2020).
53. Meyer, C. T. et al. Quantifying drug combination synergy along potency and efficacy axes. *Cell Syst.* **8**, 97–108 (2019).
54. Widge, A. T. et al. Durability of responses after SARS-CoV-2 mRNA-1273 vaccination. *N. Engl. J. Med.* **384**, 80–82 (2021).
55. McMahan, K. et al. Correlates of protection against SARS-CoV-2 in rhesus macaques. *Nature* **590**, 630–634 (2021).
56. Sette, A. & Crotty, S. Adaptive immunity to SARS-CoV-2 and COVID-19. *Cell* **184**, 861–880 (2021).
57. Wölfel, R. et al. Virological assessment of hospitalized patients with COVID-2019. *Nature* **581**, 465–469 (2020).
58. Neant, N. et al. Modeling SARS-CoV-2 viral kinetics and association with mortality in hospitalized patients from the French COVID cohort. *Proc. Natl Acad. Sci. USA* **118**, e2017962118 (2021).
59. Kissler, S. M. et al. Viral dynamics of acute SARS-CoV-2 infection and applications to diagnostic and public health strategies. *PLoS Biol.* **19**, e3001333 (2021).
60. Desikan, R., Raja, R. & Dixit, N. M. Early exposure to broadly neutralizing antibodies may trigger a dynamical switch from progressive disease to lasting control of SHIV infection. *PLoS Comput. Biol.* **16**, e1008064 (2020).
61. Yu, J. et al. DNA vaccine protection against SARS-CoV-2 in rhesus macaques. *Science* **369**, 806–811 (2020).
62. Yang, S., Jerome, K. R., Greninger, A. L., Schiffer, J. T. & Goyal, A. Endogenously produced SARS-CoV-2 specific IgG antibodies may have a limited impact on clearing nasal shedding of virus during primary infection in humans. *Viruses* **13**, 516 (2021).
63. van Gils, M. J. & Sanders, R. W. In vivo protection by broadly neutralizing HIV antibodies. *Trends Microbiol.* **22**, 550–551 (2014).
64. Fajnzylber, J. et al. SARS-CoV-2 viral load is associated with increased disease severity and mortality. *Nat. Commun.* **11**, 5493 (2020).
65. Arnaout, R. et al. SARS-CoV2 testing: the limit of detection matters. Preprint at *bioRxiv* https://doi.org/10.1101/2020.06.02.131144 (2020).
66. Gonçalves, A. et al. Timing of antiviral treatment initiation is critical to reduce SARS-CoV-2 viral load. *CPT Pharmacometrics Syst. Pharm.* **9**, 509–514 (2020).
67. Goyal, A., Cardozo-Ojeda, E. F. & Schiffer, J. T. Potency and timing of antiviral therapy as determinants of duration of SARS-CoV-2 shedding and intensity of inflammatory response. *Sci. Adv.* **6**, eabc7112 (2020).
68. Dagan, N. et al. BNT162b2 mRNA COVID-19 vaccine in a nationwide mass vaccination setting. *N. Engl. J. Med.* **384**, 1412–1423 (2021).
69. Walsh, E. E. et al. Safety and immunogenicity of two RNA-based COVID-19 vaccine candidates. *N. Engl. J. Med.* **383**, 2439–2450 (2020).
70. Anderson, E. J. et al. Safety and immunogenicity of SARS-CoV-2 mRNA-1273 vaccine in older adult. *N. Engl. J. Med.* **383**, 2427–2438 (2020).
71. Maisonnasse, P. et al. COVA1-18 neutralizing antibody protects against SARS-CoV-2 in three preclinical models. *Nat. Commun.* **12**, 6097 (2021).
72. Chigutsa, E., O'Brien, L., Ferguson-Sells, L., Long, A. & Chien, J. Population pharmacokinetics and pharmacodynamics of the neutralizing antibodies bamlanivimab and etesevimab in patients with mild to moderate COVID-19 infection. *Clin. Pharmacol. Ther.* **110**, 1302–1310 (2021).
73. Saha, A. & Dixit, N. M. Pre-existing resistance in the latent reservoir can compromise VRC01 therapy during chronic HIV-1 infection. *PLoS Comput. Biol.* **16**, e1008434 (2020).
74. Krammer, F. A correlate of protection for SARS-CoV-2 vaccines is urgently needed. *Nat. Med.* **27**, 1147–1148 (2021).
75. Chatterjee, B., Sandhu, H. S. & Dixit, N. M. The relative strength and timing of innate immune and CD8 T-cell responses underlie the heterogeneous outcomes of SARS-CoV-2 infection. Preprint at *medRxiv* https://doi.org/10.1101/2021.06.15.21258935 (2021).
76. Padmanabhan, P., Garaigorta, U. & Dixit, N. M. Emergent properties of the interferon-signalling network may underlie the success of hepatitis C treatment. *Nat. Commun.* **5**, 3872 (2014).

77. Perelson, A. S. & Ke, R. Mechanistic modeling of SARS-CoV-2 and other infectious diseases and the effects of therapeutics. *Clin. Pharmacol. Ther.* **109**, 829–840 (2020).
78. Baum, A. et al. Antibody cocktail to SARS-CoV-2 spike protein prevents rapid mutational escape seen with individual antibodies. *Science* **369**, 1014–1018 (2020).
79. Padmanabhan, P. & Dixit, N. M. Modeling suggests a mechanism of synergy between hepatitis C virus entry inhibitors and drugs of other classes. *CPT Pharmacometrics Syst. Pharm.* **4**, 445–453 (2015).
80. Chou, T. C. Theoretical basis, experimental design, and computerized simulation of synergism and antagonism in drug combination studies. *Pharm. Rev.* **58**, 621–681 (2006).
81. Padmanabhan, P., Desikan, R. & Dixit, N. M. Targeting TMPRSS2 and Cathepsin B/L together may be synergistic against SARS-CoV-2 infection. *PLoS Comput. Biol.* **16**, e1008461 (2020).
82. Brouwer, P. J. M. et al. Potent neutralizing antibodies from COVID-19 patients define multiple targets of vulnerability. *Science* **369**, 643–650 (2020).
83. Kim, K. S. et al. A quantitative model used to compare within-host SARS-CoV-2, MERS-CoV and SARS-CoV dynamics provides insights into the pathogenesis and treatment of SARS-CoV-2. *PLoS Biol.* **19**, e3001128 (2021).
84. Zarnitsyna, V. I. et al. Mathematical model reveals the role of memory CD8 T cell populations in recall responses to influenza. *Front. Immunol.* **7**, 165 (2016).
85. Benotmane, I. et al. Biomarkers of cytokine release syndrome predict disease severity and mortality from COVID-19 in kidney transplant recipients. *Transplantation* **105**, 158–169 (2021).
86. Ke, R. et al. Daily sampling of early SARS-CoV-2 infection reveals substantial heterogeneity in infectiousness. Preprint at *medRxiv* https://doi.org/10.1101/2021.07.12.21260208 (2021).
87. Golob, J. L., Lugogo, N., Lauring, A. S. & Lok, A. S. SARS-CoV-2 vaccines: a triumph of science and collaboration. *JCI Insight* **6**, e149187 (2021).
88. Zhang, Y. et al. Safety, tolerability and immunogenicity of an inactivated SARS-CoV-2 vaccine in healthy adults aged 18–59 years: a randomised, double-blind, placebo-controlled, phase 1/2 clinical trial. *Lancet Infect. Dis.* **21**, 181–192 (2021).
89. Jackson, L. A. et al. An mRNA vaccine against SARS-CoV-2—preliminary report. *N. Engl. J. Med.* **383**, 1920–1931 (2020).
90. Padmanabhan, P., Desikan, R. & Dixit, N. M. COVID-19 vaccine efficacies. *Zenodo* https://doi.org/10.5281/zenodo.5879304 (2022).

Acknowledgements

This work was supported by the DBT/Wellcome Trust India Alliance Senior Fellowship IA/S/14/1/501307 to N.M.D.

Author contributions

P.P. provided conceptualization, carried out investigations and formal analysis, contributed to writing the original draft and reviewed and edited the manuscript. R.D. performed formal analysis and reviewed and edited the manuscript. N.M.D. provided conceptualization, contributed to writing the original draft and reviewed and edited the manuscript.

Competing interests

The authors declare no competing interests.

Additional information

Supplementary information The online version contains supplementary material available at https://doi.org/10.1038/s43588-022-00198-0.

Correspondence and requests for materials should be addressed to Pranesh Padmanabhan or Narendra M. Dixit.

Peer review information *Nature Computational Science* thanks Joshua T. Schiffer and the other, anonymous, reviewer(s) for their contribution to the peer review of this work. Primary Handling Editor: Ananya Rastogi, in collaboration with the *Nature Computational Science* team.